Separation and Purification Technology 279 (2021) 119684

Contents lists available at ScienceDirect

Separation and Purification Technology

journal homepage: www.elsevier.com/locate/seppur

Highly dispersed β-FeOOH nanocatalysts anchored in confined membrane pores for simultaneously improving catalytic and separation performance

Longfei Zhang [1], Na Yang [1], Yuhang Han, Xiang Wang, Luhong Zhang, Yongli Sun, Bin Jiang [*]

School of Chemical Engineering and Technology, Tianjin University, Tianjin 300072, PR China

ARTICLE INFO

Keywords:
β-FeOOH
Heterogeneous catalysts
Peroxymonosulfate
Catalytic membrane
Confinement pores

ABSTRACT

Heterogeneous advanced oxidation process performs a promising perspective in the field of refractory pollutant degradation. However, the agglomeration and difficulty-to-recycle characters of the heterogeneous catalysts greatly impede its further development. In this study, membrane-confined pores were employed as the immobilization support to anchor highly dispersed β-FeOOH via an *in situ* mineralization method, which not only exposed highly active sites for refractory pollutants degradation but also endowed the membrane with hydrophilic/underwater superoleophobic properties. Accordingly, the Polyvinylidene fluoride/β-FeOOH (PVDF/β-FeOOH) catalytic membrane demonstrated favorable separation capacity and attractive catalytic oxidation performance via activating peroxymonosulfate. Instantaneous degradation (contact time about 1 s) of recalcitrant pollutants (over 98%) and high oil rejections (96.4% to 99.1%) can be achieved simultaneously under low operating pressure. Both the confined pore structure-induced enhanced mass transfer and enrichment of radicals and pollutants lead to favorable catalytic degradation performance. The mechanism of the catalytic membrane was analyzed by radical quenching test and electron paramagnetic resonance analysis, proving that sulfate radicals were predominant reactive oxygen species during catalytic oxidation. Besides, the PVDF/β-FeOOH catalytic membrane also possessed attractive stability without tedious catalyst separation/recovery processes. This work provides a meaningful tactic to further enhance the catalytic oxidation performance of catalytic membrane in water treatment.

1. Introduction

The worsening water pollution caused by emerging contaminants (e.g. dyes, pharmaceuticals, pesticides) has posed a great threat to the aquatic ecosystem and human health [1,2]. Extensive efforts have been devoted to eliminating environmental pollution. Effective methods such as adsorption, biological treatment, advanced oxidation processes, etc. are widely employed in the removal of the small organic matter in wastewater [3–5]. Nowadays, aiming at the effective mineralization of dissolved organic contaminants, sulfate radical based advanced oxidation processes (SR-AOPs) demonstrate superior degradation ability toward small organic pollutants [6,7]. Through the heterolysis of the -O-O- bond in peroxymonosulfate (PMS) by a range of the activation methods, sulfate radicals ($SO_4^{\cdot-}$) can be generated to attack aqueous pollutants, thereby achieving wastewater decontamination [2]. Various functional heterogeneous catalysts (e.g. transition metal oxides, activated carbon, metal–organic framework, etc.) are prevalently investigated to further improve catalytic degradation efficiency [8–10]. However, the agglomeration of the catalysts significantly impedes catalytic performance. Besides, heterogeneous catalysts require an additional separation process to realize re-utilization, which remains a critical obstacle limiting its further development [11,12].

Integrating membrane technology with AOPs to form a catalytic membrane provides an effective immobilization method for heterogeneous catalysts, thus alleviating the agglomeration of the heterogeneous catalysts to some extent by anchoring them in the membrane matrix [13–15]. In this regard, the presence of the catalysts in membrane structure enables the membrane with catalytic oxidation performance toward dissolved organic pollutants without tedious catalyst separation/recovery processes [16,17]. Besides, the membrane structure can be also optimized by employing heterogeneous catalysts as the additive and thereby affecting the separation capacity [18–20]. More importantly, tortuous channels provided by confined membrane porous structure offer abundant loading sites for catalysts and can increase the contact

* Corresponding author.
E-mail address: binj@tju.edu.cn (B. Jiang).
[1] These authors contribute equally to this work.

https://doi.org/10.1016/j.seppur.2021.119684
Received 3 August 2021; Received in revised form 2 September 2021; Accepted 6 September 2021
Available online 8 September 2021
1383-5866/

probability of the generated radicals and pollutants under enhanced mass transfer, which further accelerate the pollutants degradation process [21,22]. Furthermore, the continuous outflow of the feed stream could rapidly eliminate the intermediate products from the catalytic membrane under various operating pressures [14]. In other words, pollutants can be effectively degraded and removed from the catalyst surface under continuous operation, which significantly increases the stability and catalytic performance of the catalysts. On account of the synergy of membrane filtration and catalytic oxidation, deep decontamination of wastewater can be achieved by selective separation and small organic pollutant degradation [23,24]. Extensive efforts have been employed to optimize the structure and performance of catalytic membranes [25–27]. For instance, Wang et al. fabricated a CuO coated ceramic hollow fiber membrane which exhibited excellent bisphenol A (BPA) degradation performance in the presence of humic acid by activating PMS [13]. Ye et al. loaded ZIF-67 derived carbon frameworks on Polyvinylidene fluoride (PVDF) membrane for highly efficient BPA degradation [28]. Wang et al. enabled Ni-Co alloy and N-doped carbon nanotubes to form the catalytic membrane, which realized the degradation of emerging contaminants [29]. However, the as-prepared catalysts generally consume various organic solvents and require complicated preparation processes with high energy consumption, which poses a potential threat to the environment. Besides, heterogeneous catalysts are often embedded in membrane matrix with unsatisfied distribution, especially in the catalytic membrane prepared by phase change method or calcination process, which shelters the active sites and resulting in decreased catalytic efficiency [24]. More importantly, the synergy of catalytic degradation and selective separation of the catalytic membrane has not been comprehensively investigated since they are discussed separately to evaluate the membrane performance in most works [30–32]. Therefore, employing an eco-friendly and effective method to realize the uniform construction of heterogeneous catalysts in membrane support to further enhance catalytic performance is of great importance.

Iron-based catalysts are widely employed in the field of activating PMS to degrade organic pollutants due to their high catalytic activity and eco-friendly characters [33–35]. Among them, iron oxyhydroxide (FeOOH) with abundant surface hydroxyl groups, favorable hydrophilicity, and high catalytic performance has caused widespread attention [36–38]. Owing to the controlled preparation method, β-FeOOH generated by *in situ* mineralization of Fe^{3+} ions is often utilized to form hybrid catalysts to realize Fenton-like reactions without complicated synthesis processes [37]. For example, Lyu et al. loaded β-FeOOH on MnO_2 support as the PMS activator and demonstrated favorable catalytic degradation performance toward Acid orange 7 [39]. Wang et al. enabled *in situ* growth method to anchor β-FeOOH on g-C_3N_4, which can be employed to achieve deep oxidation of the emerging contaminants via activating PMS [38]. However, the severe agglomeration and inferior recyclability of the suspended β-FeOOH nanoparticle restrict its further application. Herein, the combination of β-FeOOH and membrane can be regarded as a win–win strategy, which can fully exert the catalytic performance of the catalysts and endow the membrane with optimized hydrophilicity to enhance separation capacity.

In this study, highly dispersed β-FeOOH was anchored in PVDF confined membrane pores via an *in situ* mineralization method to realize the uniform distribution of heterogeneous catalysts in membrane structure. The tortuous channels in membrane structure provide abundant reaction sites for the reactive oxidation species and pollutants under enhanced mass transfer, which is beneficial to fulfill the catalytic performance. Besides, the selective separation of the membrane was also optimized by the homogeneous distribution of heterogeneous catalysts with favorable hydrophilicity. The structure and morphology of the catalytic membrane were analyzed. The catalytic degradation and selective separation performance of the membrane was researched systematically. Moreover, the influences of the operating parameters and various conditions on the catalytic performance of the catalytic membrane were analyzed in detail. Finally, the stability, mechanism, and degradation pathways of the pollutants were also evaluated.

2. Experimental

2.1. Chemical and reagents

Iron chloride hexahydrate ($FeCl_3{\cdot}6H_2O$, 99%), hydrochloride acid (HCl, 36.0–38.0%), methanol (MeOH, 99%), Rhodamine B (RhB, 99%), Methylene orange (MO, 99%), and Congo red (CR, 99%) were obtained from Kermel Chemical Reagent Co., Ltd. (Tianjin, China). Peroxymonosulfate ($2KHSO_5{\cdot}KHSO_4{\cdot}K_2SO_4$, AR grade), *tert*-butyl alcohol (TBA, 99%), and sodium dodecylsulfate (SDS) were purchased from Aladdin Chemistry Co., Ltd (Shanghai, China). Commercial PVDF membranes (pore size of 0.1 μm) were purchased from Zhongli Filtration Co., Ltd. (Haining, China). All chemicals were used without further purification. Deionized water was used throughout the experiment.

2.2. Fabrication of β-FeOOH on confined PVDF membrane pores

The commercial PVDF membrane was cut to an appropriate size (≈ 5 cm^2) and immersed in ethanol for 2 h to remove impurities. Then, PVDF membrane was washed by deionized water several times and soaked in a beaker containing 20 mL $FeCl_3{\cdot}6H_2O$ (18 mg/mL) and 10 mL HCl (10 mM). Afterwards, the above system was transferred to a 60 °C oven to complete the *in situ* mineralization process (mineralization time was 6, 12, 18, and 24 h, respectively). During this procedure, Fe^{3+} was converted to β-FeOOH and anchored in membrane confined pore structure and connected with the inner pores of the membrane. The color of the membrane turned from white to pale yellow. Finally, the PVDF/β-FeOOH catalytic membrane was rinsed by deionized water several times and dried prior to use. The loading amount of the β-FeOOH was measured by the weight change before and after mineralization process.

2.3. Analytical methods

The morphology and structure of membranes were characterized by scanning electron microscope (SEM, Hitachi S4800, Japan), and the element distribution was measured by energy dispersive spectrometer (EDS). The surface roughness of the membrane was evaluated by atomic force microscopy (AFM, Bruker, Dimension icon, Germany). X-ray diffractometer (XRD, D8 Bruker-AXS, Germany) was employed to analyze the crystal structure of the membranes. X-ray photoelectron spectrometer (XPS, ESCALAB 250Xi, UK) was used to verify the surface component and valance state of the membrane. The water contact angle (WCA) and underwater oil contact angle (UOCA) of the membrane were measured by contact angle equipment (Powereach, China), briefly, five kinds of oil containing gasoline, soybean oil, n-hexane, petroleum ether, and dichloromethane were employed to test the UOCA of the membrane. The electron paramagnetic resonance (EPR, EMXPLUS, German) was introduced to verify the generation of the radicals by using 5, 5-dimethyl-1-pyrroline-N-oxide (DMPO) as the spin-trapping agent. The intermediate products of RhB degradation were identified by ultra-high-performance liquid chromatography-mass spectrum (UHPLC-MS, Thermo Vanquish UHPLC-LTQ XL, USA). Besides, the mineralization rate of the target pollutant was tested by a total organic analyzer (TOC-L, Shimadzu, Japan).

2.4. Performance evaluation of PVDF/β-FeOOH catalytic membranes

Cross-flow apparatus was used to evaluate the performance of PVDF/β-FeOOH catalytic membranes throughout the experiment. The flux of the membranes was measured by Eq. (1).

$$F = \frac{V}{A \times t} \tag{1}$$

where F is the water flux of membrane ($L{\cdot}m^{-2}{\cdot}h^{-1}$), V represents the volume of the permeate (L), A is the effective area of membrane (4.9 cm^2), and t means the operation time.

The porosity of the membrane was measured by Eq. (2).

$$\varepsilon = \frac{W_w - W_d}{\rho_w A \delta} \tag{2}$$

where ε is the porosity of membrane (%), W_w and W_d are the wet and dry weight of membranes (g), ρ_w means the density of deionized water (g/cm^3), A is the effective area of membrane (4.9 cm^2), and δ means the thickness of the membrane (cm).

To investigate the separation performance of the membrane, oil-in-water emulsions were prepared by mixing 1 g oil (gasoline, soybean oil, n-hexane, petroleum ether, and dichloromethane) and 0.1 g SDS into 1 L deionized water. A homogenizer (FLUKO FA25, German) was employed to disperse the oil in water phase at 10000 rpm for 10 min to obtain stabilized oil-in-water emulsion [40]. The separation performance of the membrane was elucidated through Eq. (3).

$$R = \frac{C_o - C}{C_0} \times 100\% \tag{3}$$

where R means the oil rejection (%). C_0 and C are the oil concentrations of initial and permeate oil-in-water emulsions (mg/L), which were analyzed by the total organic analyzer and infrared spectrometer oil content analyzer (CY2000, China).

The anti-fouling capacity of the membrane was also investigated. In a typical process, the membrane was pre-compacted by deionized water at 0.12 MPa for 30 min. Then, decreasing the operation pressure to 0.1 MPa, the pure water flux (J_1) was tested and recorded. After that, deionized water was replaced by the above-mentioned simulated wastewater for another 30 min. The fouled membrane was cleaned by PMS aqueous solution (1 mM) backwashing 15 min and the recuperated water flux was recorded (J_2). The above process was repeated three times, and the flux recovery rate (FRR) was calculated by Eq. (4).

$$FRR = \frac{J_2}{J_1} \times 100\% \tag{4}$$

Taking RhB removal as the indicator, the catalytic performance of the PVDF/β-FeOOH membrane was systematically analyzed. Briefly, 500 mL 10 ppm RhB solution was carried out in a feed tank and several amounts of PMS were introduced during the operation process. It is worth noting that the permeate solution was separated from the system and the feed stream was calculated continuously. Periodically, the sample was withdrawn from the permeate solution and evaluated by an ultraviolet–visible spectroscopy (UV–vis 4802S, Unico, USA) at the wavelength of 554 nm. Besides, the degradation ability of other refractory pollutants (CR and MO) was also involved to test the catalytic activity of the membrane. The influences of various parameters (operating pressure, pH, and temperature, etc.) were also researched. The radical quenching test was also employed to analyze the mechanism of catalytic oxidation and the species of the radicals. To further verify the synergy of membrane separation and catalytic oxidation, simulated wastewater containing various oil-in-water emulsions and RhB was treated by the membrane, and the separation and catalytic degradation efficiency were analyzed. The influences of the oil-in-water emulsion concentration, RhB concentration, and operating pressure were investigated. Furthermore, the stability of the membrane was tested by

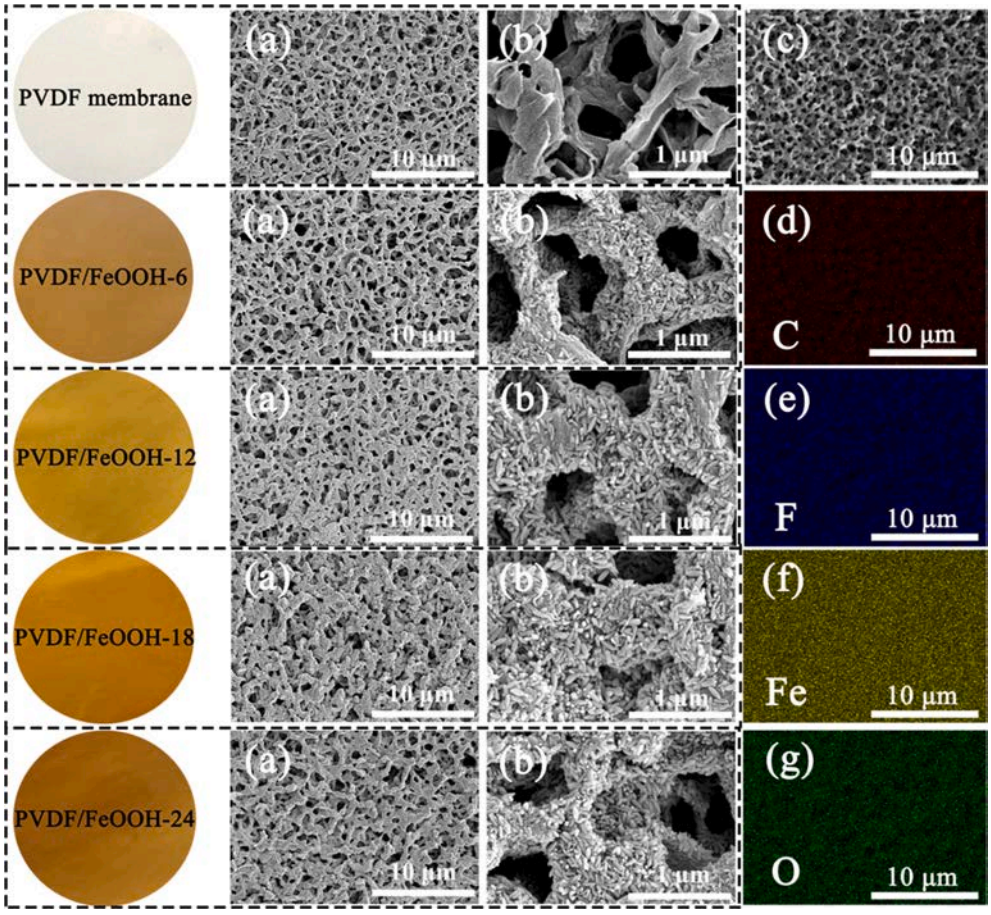

Fig. 1. Morphologies and structures of the membranes. SEM images of pristine PVDF membrane, and PVDF/β-FeOOH membrane under various mineralization time (a); enlarged surface morphology (b); EDS element mapping of PVDF/β-FeOOH-12 membrane (c-g).

treating the RhB solution for 12 h at 0.02 MPa and the permeation flux of the membrane was also recorded.

3. Results and discussion

The morphologies of the membranes are shown in Fig. 1. For the pristine PVDF membrane, the porous structure with good connectivity was observed on membrane surface, which was beneficial to improve water treatment capacity [41]. When β-FeOOH was anchored in the confined membrane pore structure, the color of the membrane changed gradually from white to orange. Abundant rod-like β-FeOOH was found on the surface and inside pore structure of the membrane to construct a micro-nano hierarchical structure on membrane surface [37]. The β-FeOOH size gradually increased and covered membrane structure with the increment of mineralization time, resulting in a narrower pore size distribution. Besides, on account of the uniformly anchored β-FeOOH on confined hierarchical membrane pore structure, the contact probability of the generated radicals and pollutants increased significantly in membrane channels, thus further accelerating the pollutants degradation process [14,21,42]. EDS mapping was employed to further analyze the surface composition of the membranes (Fig. S1). As described in Fig. 1 (c-g), it can be observed that the C, F, Fe, and O elements distributed evenly on membrane surface, validating the formation of the highly dispersed β-FeOOH nanocatalysts.

The XRD patterns of the membrane are depicted in Fig. 2(a). It was observed that the pristine PVDF membrane exhibited a semi-crystalline structure [14]. For the β-FeOOH decorated PVDF membrane, the characteristic peaks situated at $2\theta = 11.8°$, 26.7°, 35.2°, 39.2°, 46.4°, and 56.0° corresponded to the (110), (310), (211), (301), (411), and (521) planes, which well-matched the PDF card (No. 34–1266), confirming the anchoring of β-FeOOH on PVDF membrane [43,44]. The peak intensity of β-FeOOH increased along with the mineralization process [45]. Besides, no other iron oxides were identified from the XRD pattern. Fig. 2(b) displayed the full-scale XPS spectrum of the PVDF and PVDF/β-FeOOH-12 membrane. Compared with the pristine PVDF membrane, two new peaks of Fe 2p and O 1s appeared while the peak intensity of F 1s significantly lessened, demonstrating the formation of β-FeOOH on membrane structure. High resolution Fe 2p spectrum was conducted to further verify the composition of β-FeOOH and is described in Fig. 2(c). Two main peaks located at 710.8 and 724.5 eV were assigned to Fe $2p_{3/2}$ and Fe $2p_{1/2}$ region. Besides, two satellites were also observed, which proved the mixed valance of the β-FeOOH [37,46]. The peaks at 711.8 and 725.7 eV were referring to the existence of Fe^{3+} while that at 710.2 and 723.9 eV corresponded to Fe^{2+} [9,38]. The overall ratio of Fe^{3+} to Fe^{2+} was calculated as 1.48, indicating that Fe^{3+} was predominated in β-FeOOH. As shown in Fig. 2(d), the core-level O 1s spectrum mainly divided into three peaks which corresponded to lattice oxygen $Fe\text{-}O_2^-$ (529.5 eV), Fe-O bond (531.1 eV) of the β-FeOOH, and the adsorbed H_2O and CO_2 on β-FeOOH surface (532.7 eV), respectively [37,47]. Based on the O 1s deconvolution spectrum, $Fe\text{-}O_2^-$, Fe-O and adsorbed H_2O and CO_2 accounted for 24.8%, 60.5%, and 14.7% respectively. Apparently, the relatively high proportion of adsorbed H_2O

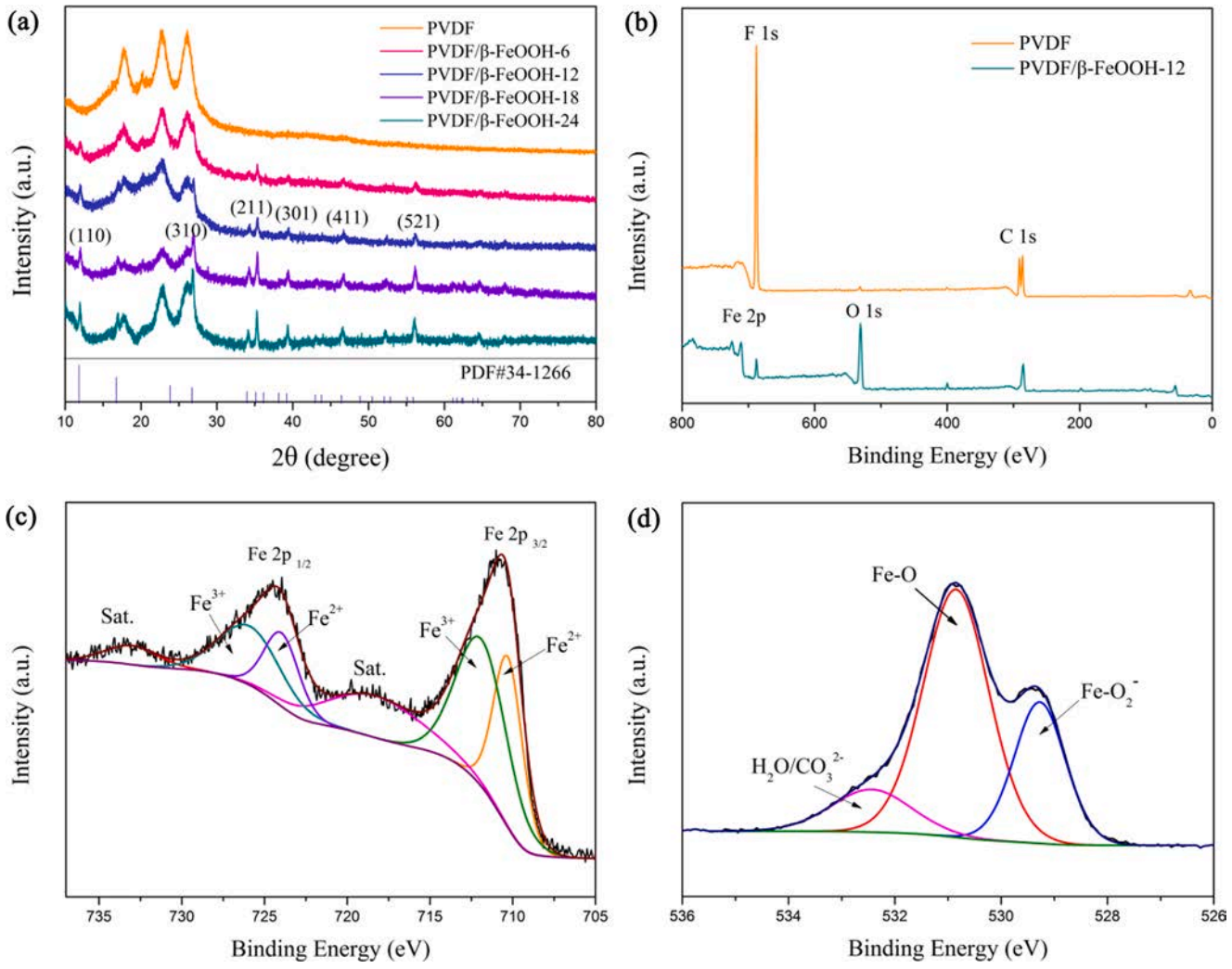

Fig. 2. XRD patterns of the membrane (a); full-scan XPS spectrum (b); high resolution spectrum of Fe 2p (c) and O 1s of PVDF/β-FeOOH-12 membrane (d).

and CO_2 was attributed to the abundant hydroxyl groups on β-FeOOH structure, which can readily capture water molecular on membrane surface, thus enabling better hydrophilicity and anti-fouling performance of the membrane.

The hydrophilicity of the membrane was investigated using WCA as the indicator. As illustrated in Fig. S2, the pristine PVDF membrane presented a WCA of 122.3 ± 2.7°, which revealed the intrinsic hydrophobic characteristic of the PVDF molecular. The WCA sharply decreased to 58.1 ± 2.8°, 44.7 ± 2.3°, 40.6 ± 2.1°, and 35.9 ± 2.5° when mineralization time reached 6, 12, 18, and 24 h respectively, manifesting better hydrophilicity owing to the existence of the hydroxyl groups on β-FeOOH surface. As the mineralization progress processed, the loading amount of β-FeOOH gradually rose, which was able to furnish more hydroxyl groups on membrane surface and resulted in the descending trend of WCA. In addition, the loading amount of β-FeOOH on PVDF membrane is summarized in Table S1, and the effective area is 5 cm^2. The results showed that β-FeOOH was successfully loaded on PVDF membrane (about 2.5, 4.3, 7.4, and 9.7 mg for the mineralization time of 6, 12, 18, and 24 h, respectively), and thus changing the surface properties of the membrane. To further verify the surface properties, five different types of oil were employed to reveal the repellency of membrane surface to oil droplets (Fig. 3). The UOCA of 110.4 ± 1.2°, 126.4 ± 1.5°, 112.7 ± 0.8°, 140.5 ± 1.9°, and 114.5 ± 2.8° was observed for PVDF membrane corresponded to gasoline, soybean oil, n-hexane, petroleum ether, and dichloromethane, respectively, while that for PVDF/β-FeOOH-12 membrane was 154.1 ± 1.4°, 152.3 ± 2.1°, 154.8 ± 2.0°, 158.6 ± 1.7°, and 157.5 ± 2.1°. The increment of the UOCA of PVDF/β-FeOOH-12 membrane elucidated underwater superoleophobic properties with the aid of uniformly anchored β-FeOOH on confined membrane pores, which further enhanced the separation performance of the membrane [48].

The surface roughness of the membrane was analyzed by AFM and shown in Fig. 4, owing to the micro-nano hierarchical structure formed on membrane surface, the Ra of the membrane decreased from 180.0 to 55.9 nm, indicating the uniform distribution of β-FeOOH on membrane surface. Lower roughness was conducive to enable better anti-fouling performance, which further enhanced the recyclability of the membrane [37].

The permeability and separation performance is imperative to verify the water treatment capacities of the membrane [49,50]. However, owing to the intrinsic hydrophobic character of the pristine PVDF membrane, ethanol pre-wetting should be carried out prior to water flux testing. As illustrated in Fig. 5(a), the water flux of the membrane improved initially and followed with a downward trend along with the mineralization time. Maximum of 4097.9 L/m^2h of water flux can be reached when mineralization time was 12 h. The uniformly anchored β-FeOOH was beneficial to increase the hydrophilicity and led to the increment of the water flux. However, with the prolonging of mineralization time, excess distributed β-FeOOH led to a narrower pore size, which caused the decline of water flux concomitantly. Consistent with the speculation, the porosity of the membrane also reduced with the increase of mineralization time. PVDF/β-FeOOH-12 membrane was chosen as the optimal membrane because of the relatively high water flux and RhB degradation efficiency (Fig. S3) and was employed to further demonstrate the separation performance. As illustrated in Fig. 5 (b), the oil flux weakened evidently because of the membrane fouling caused by the adhesion of the high dispersed oil droplet on membrane surface, and maintained 232.6, 220.4, 239.3, 244.9, and 230.6 L/m^2h for gasoline, soybean oil, n-hexane, petroleum ether, and dichloromethane, respectively. Besides, given the improved hydrophilicity, high oil rejections were achieved for diverse oils, which were 96.4%, 97.6%, 96.8%, 97.1%, and 99.1%, respectively, while that for pristine PVDF membrane was about 60 %. Optical microscope was employed to reveal the oil rejection performance and the results are shown in Fig. S4. In summary, the uniformly anchored β-FeOOH in confined membrane pores not only improved the permeability but also intensified the separation performance of the membrane, which provided a prerequisite for its further application in the field of catalytic oxidation.

The catalytic performance of the membrane was carried out in a cross-flow filtration mode. It should be noticed that the permeation was separated from the system while the feed stream was continuously circulated in the feed tank during the whole degradation process. In a typical run, 500 mL 10 ppm RhB was employed as the target pollutant and a certain amount of PMS was introduced into the above-mentioned solution. Afterwards, the RhB solution was circulated through the system, and the permeation sample was withdrawn in a certain time interval and test by UV-spectrum to verify the RhB degradation performance. The correlative relationship between operating pressure and flux is depicted in Table S2. As shown in Fig. 6(a), both PVDF and PVDF/β-FeOOH-12 membrane exhibited limited adsorption capacity toward RhB. Owing to the increased hydrophilicity and declined porosity, the hydrophobic interaction between membrane and pollutants was restricted. Only 7.2 % of RhB was rejected through the PVDF/β-FeOOH-12 membrane, indicating a lower RhB adsorption ability. Besides, 8.4 % of the RhB was degraded in the pure PMS-dominated degradation process, implying the weak self-decomposition properties in the presence of PMS alone. Nevertheless, the presence of PMS and membrane significantly altered this phenomenon. For the RhB removal in PVDF/PMS system, a fascinating phenomenon occurred. The results showed that about 84.3% of RhB was removed in the first 3 min, but declined sharply to 43.9% at 30 min. The reason can be explained by the synergistic effect of adsorption and the increment collision probability of the PMS and pollutants induced by confined membrane pore structure [14,21]. In other words, sufficient contact between radicals and pollutants can be achieved when the fluid passed through the curved channels in membrane structure, resulting in a boosted RhB removal in the initial stage. However, with the continuous accumulation of the RhB in membrane structure, pure PMS dominated RhB degradation process became pale and weak, thus demonstrated a deteriorated RhB removal efficiency as the catalytic oxidation proceeded. When PVDF/β-FeOOH-12 membrane was employed to treat RhB solution, RhB decolorized immediately when it passed through the membrane. Over 99% of RhB was removed, indicating a superior catalytic efficiency. The diminished adsorption peak at about 554 nm further proved the rapid degradation

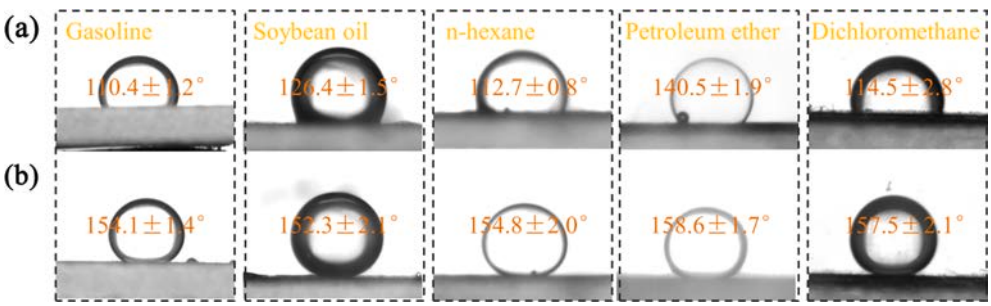

Fig. 3. Various UOCA of pristine PVDF membrane (a) and PVDF/β-FeOOH-12 membrane (b).

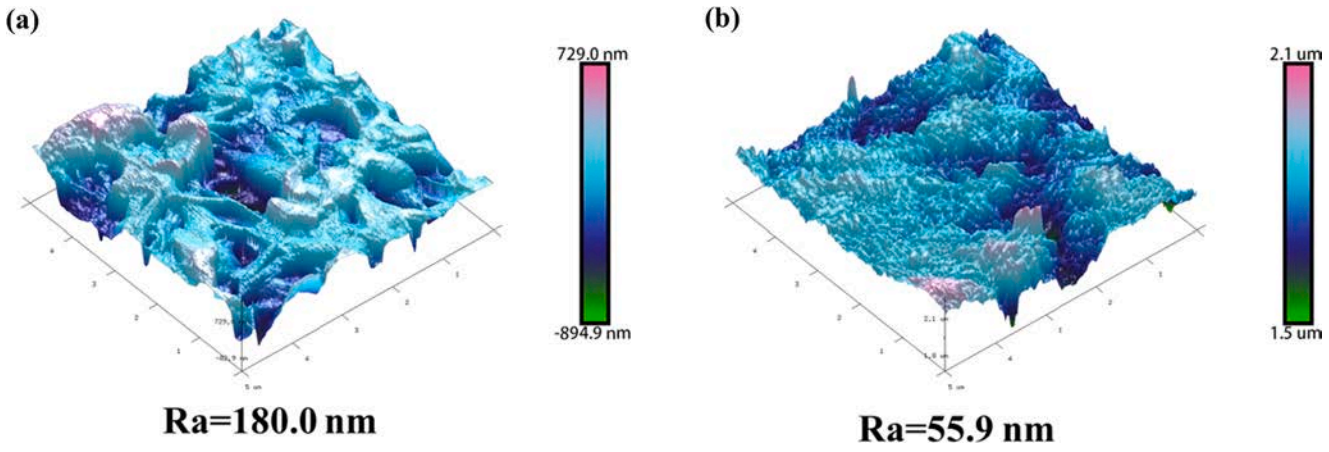

Fig. 4. Surface roughness of the pristine PVDF membrane (a) and PVDF/β-FeOOH-12 membrane.

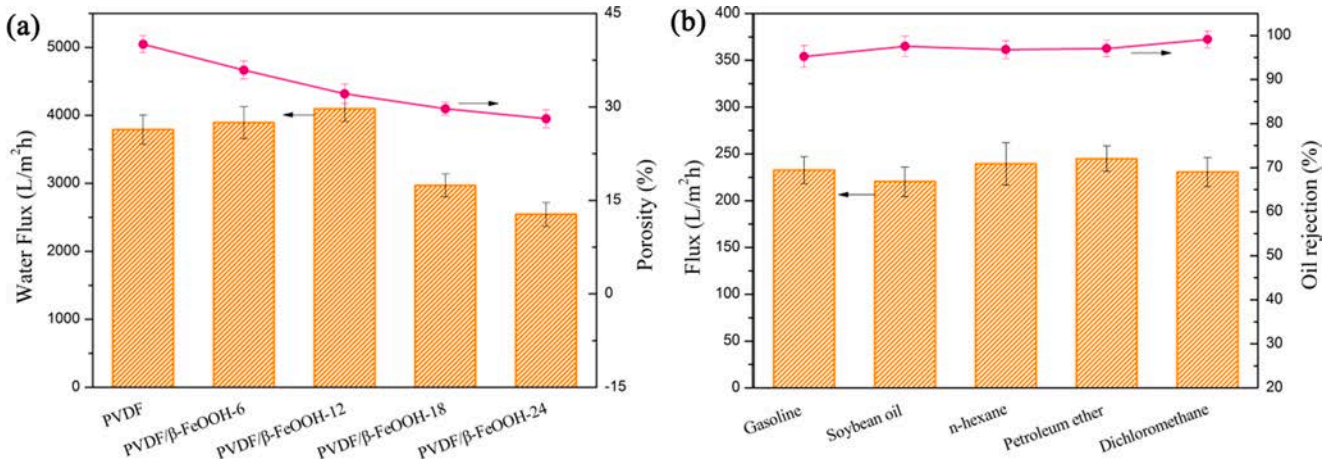

Fig. 5. Water flux and porosity (a); oil flux and rejection of PVDF/β-FeOOH-12 membrane.

of RhB through the catalytic membrane (Fig. S5). In other words, the RhB in each drop of filtrate can be degraded instantly, performing a favorable decontamination capacity toward small organic pollutants. The following two aspects can be adopted to explain the boosted catalytic efficiency. 1) The uniformly anchored β-FeOOH catalysts on membrane structure presented multiple hierarchical reaction sites for high-efficient RhB degradation; 2) concentrated pollutants and PMS-induced radicals in confined membrane pore structure were favored to increase effective contact to enhance mass transfer, and thus further improving RhB removal efficiency. Besides, the catalytic performance of the membranes in various conditions (RhB degradation in feed tank or a beaker separated from the cross-flow filtration mode, etc.) was also investigated and shown in Fig. S6. The results indicated that the catalytic membrane exhibited attractive degradation efficiency and can be identified as a reaction amplifier to further promote catalytic oxidation [14,51]. Accordingly, the contact time of the RhB and PMS in membrane can be calculated by the correlation between membrane thickness (δ) and flux (F) through the following equation since F can be regarded as the flow velocity of the membrane ($t = \delta/F$) [21]. Only 1.08 s was needed to achieve about 99% RhB degradation, demonstrating an ultrafast degradation rate. The influence of the operating pressure on RhB degradation is depicted in Fig. 6(b), it was noteworthy that the operating pressure greatly affected the flux of the RhB solution. The higher operating pressure, the lower contact time was obtained between pollutants and membrane, as well as an increased pollutants accumulation rate. Therefore, the RhB degradation was hindered to some extent as the pressure rose. But equilibrium can be gradually accomplished between pollutants accumulation and catalytic degradation owing to the continuous progress of catalytic degradation. Took for example when pressure was 0.1 MPa, about 61.4% of RhB was degraded at 21 min and maintained at about 60% until 30 min. In general, the membrane performed better degradation ability under low operation pressure, which was a more cost-effective approach to wastewater remediation. As shown in Fig. 6(c), in the presence of 0.5 mmol/L PMS, 76.6% of RhB can be degraded in 30 min, but the RhB degradation efficiency increased obviously with more addition of PMS. Therefore, 1.0 mmol/L PMS was considered as the optimal concentration and was further employed in the following experiments. Besides, the PVDF/β-FeOOH-12 membrane revealed attractive RhB degradation ability in a wide pH range from 3 to 9. However, the RhB degradation was restricted when pH reached 11 in terms of the intrinsic pK_a of PMS ($pK_{a2} = 9.4$). When pH was higher than pK_{a2}, the main component of PMS transferred to SO_5^{2-} with unsatisfied oxidation ability and exhibited a declined RhB degradation efficiency [6]. Fig. 6(e) revealed that the elevated temperature was conducive to facilitate the RhB degradation process. Rapid generation of radicals can be realized under increased temperature owing to the thermodynamic favorable character of PMS. Furthermore, Fig. 6(f) showed that the RhB degradation efficiency decreased along with the increment in pollutant concentration. The TOC removal of the RhB solution was tested and shown in Fig. S7. A certain amount of samples were separated and circulated through the catalytic membrane three times. The mineralization rates of the first, second, and third cycles were 6.5%, 10.4%, and 14.2%, respectively. Obviously, the catalytic membrane performed an attractive mineralization rate in a short reaction time, which was caused

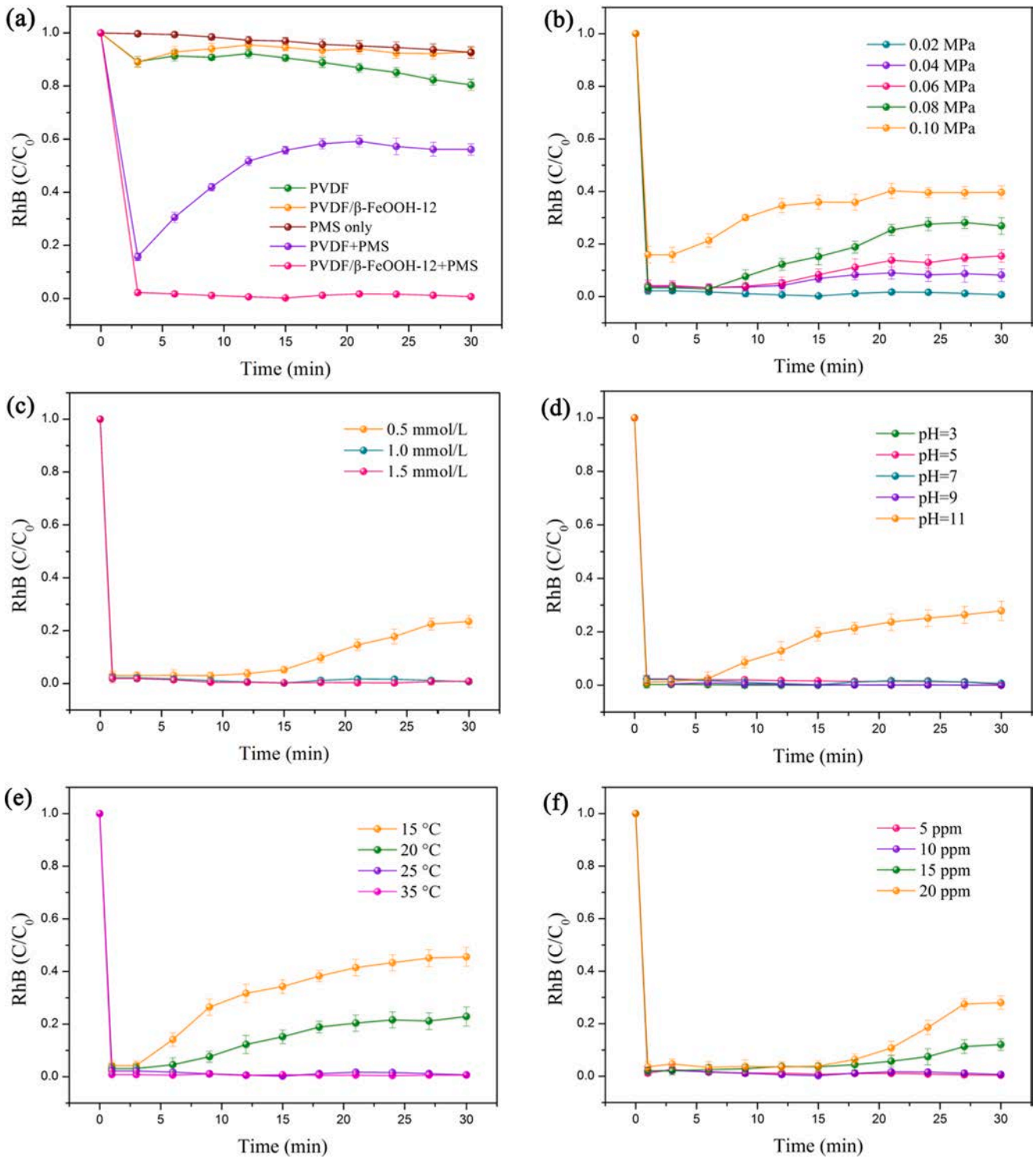

Fig. 6. Catalytic performance of the PVDF/β-FeOOH-12 membrane. Comparison of the PVDF and PVDF/β-FeOOH-12 membrane (a); effect on operation pressure (b); PMS concentration (c); pH (d); temperature (e) and pollutant concentration (f). (Operating conditions: RhB 500 mL, 10 ppm; PMS concentration: 1.0 mM; temperature: 25 °C; pressure: 0.02 MPa).

by the highly dispersed reaction sites provided by β-FeOOH and the enhanced mass transfer that occurred in confined membrane pore structure.

Through a series of investigations on the performance of PVDF/β-FeOOH-12 membrane, we found that the catalytic membrane presented attractive separation and catalytic oxidation ability respectively. To further exert the water treatment capacity, it is imperative to explore the synergistic effect of membrane separation and catalytic oxidation. Therefore, simulated wastewater containing various oil-in-water emulsions and RhB was employed to verify the performance of the membrane. Initially, to explore the effect of the external pollutants on RhB degradation, oil-in-water emulsions (soybean oil) with a range of concentration gradients and 10 ppm RhB were employed and circulated under 0.1 MPa through the PVDF/β-FeOOH-12 membrane. The results demonstrated that the concentration of external pollutants performed little effect on RhB degradation (over 98%), and the oil rejection

remained 98.6%, 98.3%, 98.0%, and 97.7% for various oil concentrations, respectively. The phenomenon can be explained from the following two aspects: 1) owing to the continuous accumulation of oil droplets on membrane surface, the permeate flux of PVDF/β-FeOOH-12 membrane decreased concomitantly (insert Fig. 7(a)). Correspondingly, lower flux represented longer contact time between pollutants and catalysts in membrane structure, and thus the membrane still maintained favorable RhB degradation performance; 2) due to the increased hydrophilicity provided by β-FeOOH, hydration layer was formed on membrane surface, and thus, the oil rejection was further promoted [16]. Therefore, the PVDF/β-FeOOH-12 membrane still maintained a high rejection for oil-in-water emulsions. On account of the high oil rejection, the oil concentration in simulated wastewater was set as 1000 ppm. The RhB degradation efficiency was monitored by adjusting RhB concentration. As depicted in Fig. 7(b), as the RhB concentration increased from 10 to 30 ppm, the degradation efficiency of RhB deteriorated to a certain extent, but still maintained 95.6% when RhB concentration was 30 ppm. The improved RhB degradation efficiency was ascribed to the declined permeate flux in the presence of oil-in-water emulsions. Therefore, by adjusting the operating pressure, the RhB degradation efficiency (1000 ppm oil-in-water emulsion and 10 ppm RhB) was investigated under different flux conditions. Under similar flux conditions compared with pure RhB solution (370 vs. 398 L/m^{2}h), the RhB degradation efficiency decreased from 99.3% to 96.1%, indicating that part of the PMS was obscured by oil droplets, and resulted in a descending trend in RhB degradation performance. Besides, the RhB elimination efficiency decreased as the flux accelerated. In other words, the combination of membrane separation and catalytic oxidation can be better guaranteed under low operation pressure, which is a more cost-effective approach to realize wastewater decontamination. Furthermore, simulated wastewater containing various oil-in-water emulsions (1000 ppm) and RhB (10 ppm) was employed to verify the performance of the membrane (Fig. 7(d)). Under the flux of ~ 220 L/m^{2}h, the contact time of the pollutants and PMS in membrane extended to 1.80 s. The results demonstrated that the membrane performed favorable RhB degradation efficiency in the presence of various oil-in-water emulsions. Instantaneous degradation of RhB was accomplished and reached 99.1%, 99.0%, 97.6%, 99.5%, and 99.4% for various oil-in-water emulsions, respectively. Moreover, the oil rejection also maintained over 97% for various oils. In this regard, the respective merits of membrane separation and catalytic oxidation were integrated positively. Therefore, through the synergistic effect of membrane separation and catalytic oxidation, the application range of the catalytic membrane can be further broadened, thus improving the water treatment capacity.

As an important index to evaluate the membrane performance, the anti-fouling ability should be investigated. Simulated wastewater containing oil-in-water emulsion (soybean oil) and RhB was employed to verify the fouling resistance to maintain the consistency of the experiment. As depicted in Fig. 8(a), the pristine PVDF membrane demonstrated unsatisfied anti-fouling performance even after the backwashing

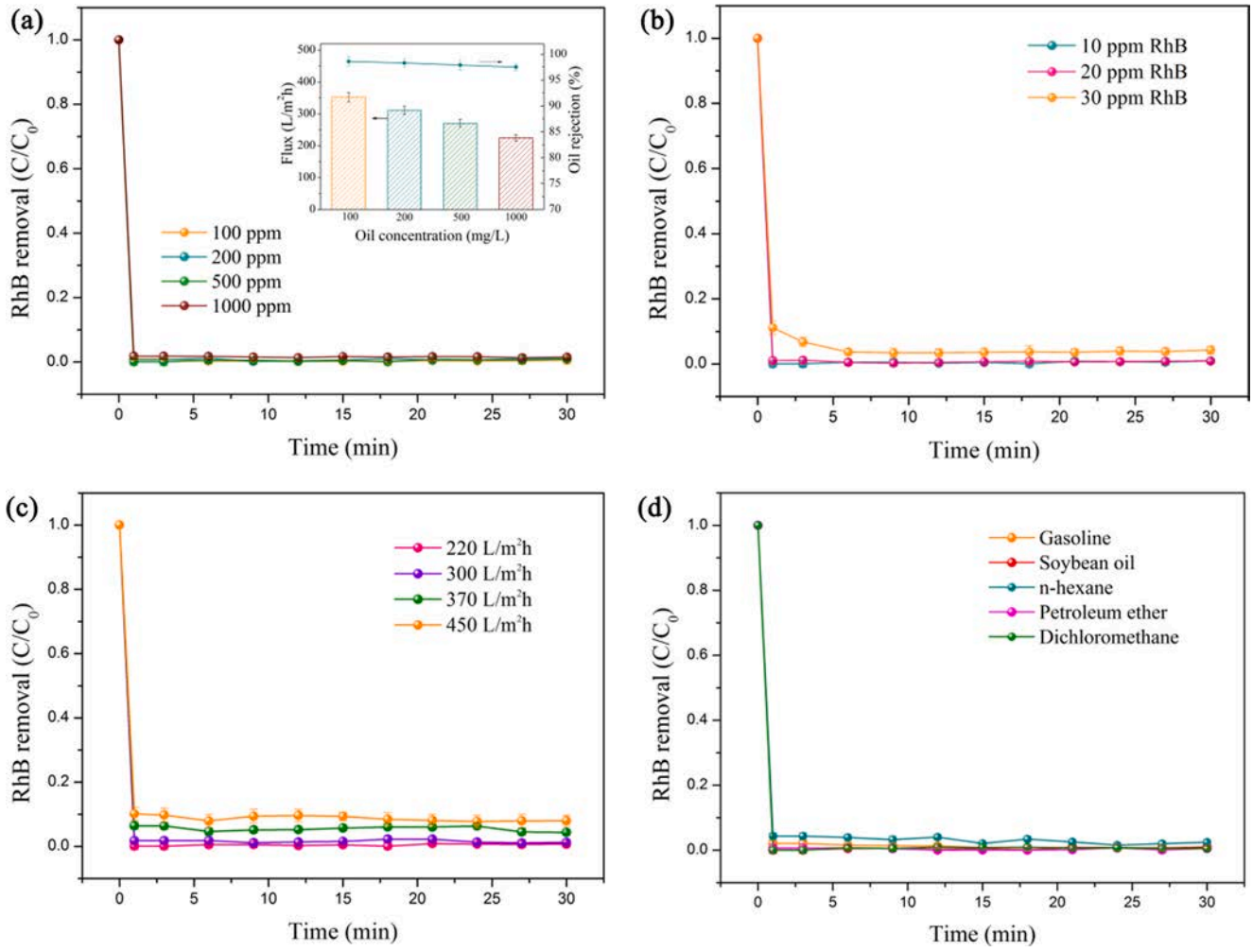

Fig. 7. Investigation on the synergy effect of PVDF/β-FeOOH-12 membrane toward simulated wastewater. Effect on oil-in-water emulsion concentrations (a) and relevant flux and oil rejections (insert a); effect on RhB concentration (b); effect of permeate flux on RhB degradation performance (c) and RhB degradation in various oil-in-water emulsions (d). (Temperature: 25 °C; PMS concentration: 1.0 mM; volume of the simulated wastewater: 500 mL).

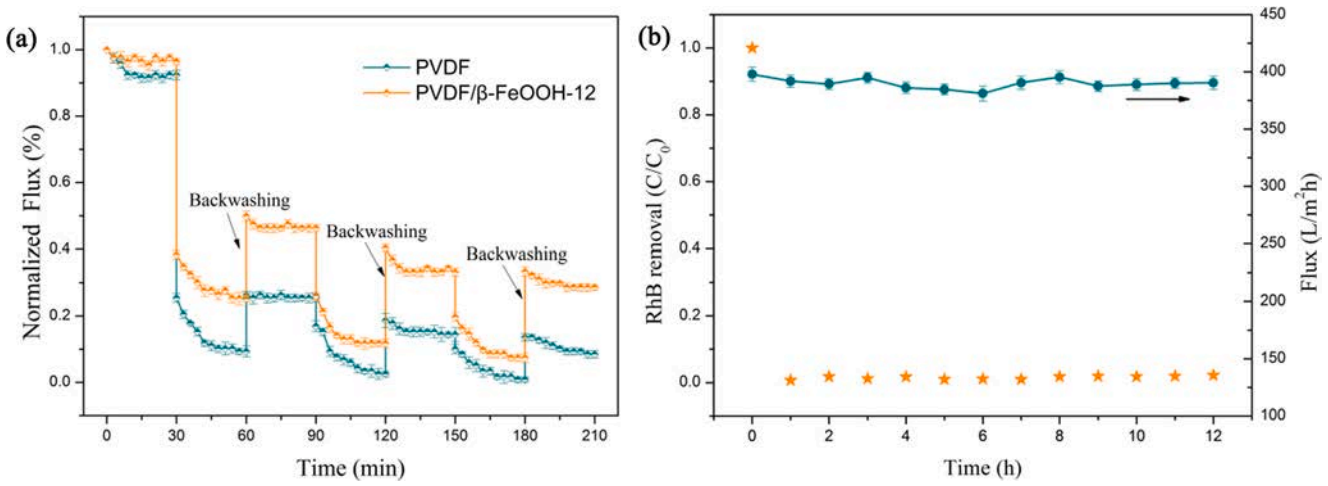

Fig. 8. Anti-fouling performance of the membrane (a) and stability test (b).

process using 1.0 mmol/L PMS solution as the cleaning agent. The FRR of the PVDF membrane sharply declined to 8.5% after three successive cycles owing to the continuous accumulation of the pollutants on membrane surface. For the PVDF/β-FeOOH-12 membrane, the descending trend was alleviated owing to the improved hydrophilicity and exhibited a higher flux than pristine PVDF membrane. Furthermore, the FRR increased to 28.7% after three times of backwashing, which could be attributed to the degradation of the pollutants on membrane surface, indicating favorable anti-fouling properties induced by PMS. The stability of the PVDF/β-FeOOH-12 membrane was also investigated and shown in Fig. 8(b), over 98% of RhB can be degraded after 12 h stability test. Besides, the flux of the PVDF/β-FeOOH-12 membrane also maintained at about 390 L/m^2h. These results indicated that the PVDF/β-FeOOH-12 membrane performed attractive stability toward organic pollutant together with the relatively stable flux. The morphology and structure of the membrane were basically unchanged after catalytic oxidation (Fig. S8), manifesting a favorable stability without tedious catalysts recycle process. Besides, the degradation performance of other small organic pollutants like MO and CR is shown in Fig. S9, vindicating the attractive degradation ability.

To identify the species of the radicals, radical quenching test was employed by using MeOH and TBA as the radical scavenger [7,52]. Fig. 9(a) revealed that the addition of 0.2 mol/L TBA (scavenger for ·OH) performed a limited effect on RhB degradation and it can still maintained relatively high degradation efficiency within 30 min. However, in the presence of 0.2 mol/L MeOH as the scavenger of both ·OH and $SO_4^{\cdot-}$, the RhB degradation efficiency gradually declined with the operating time. About 55.1% of RhB was removed at 30 min, which indicated that the $SO_4^{\cdot-}$ played a dominate role in the RhB degradation process. The generation of the radicals was further analyzed by EPR. As depicted in Fig. 9(b). Both signals of ·OH and $SO_4^{\cdot-}$ were detected in the EPR spectrum, indicating that both ·OH and $SO_4^{\cdot-}$ were involved in RhB degradation process.

To better reveal the mechanism of the catalytic oxidation, the high-resolution XPS spectrums of Fe 2p and O 1 s before and after reaction were obtained. As shown in Fig. 10(a), the location of the peaks was almost unaltered but the valance state of the Fe species changed to a certain extent. The overall ratio of Fe^{3+} to Fe^{2+} increased from 1.48 to 1.59 after catalytic oxidation, indicating that the redox pair of Fe^{3+}/Fe^{2+} was involved in PMS activation process. However, owing to the existence of the limited reaction step as Eq. (6), the generation of Fe^{2+} was hindered, and thus, resulting in the increment of Fe^{3+}/Fe^{2+} ratio. Besides, the composition of the oxygen species changed from 24.8% (Fe-O_2^-), 60.5% (Fe-O), and 14.7% (adsorbed H_2O and CO_2) to 22.9%, 54.5%, and 22.6%, respectively. The increased ratio of adsorbed H_2O and CO_2 might be attributed to the adsorption of the degradation intermediates on membrane. In this regard, the composition of Fe-O_2^- and Fe-O also decreased. To further verify the iron species involved in catalytic degradation, XRD patterns of the PVDF/β-FeOOH-12 membrane were conducted and shown in Fig. S10. The crystal structure of PVDF/

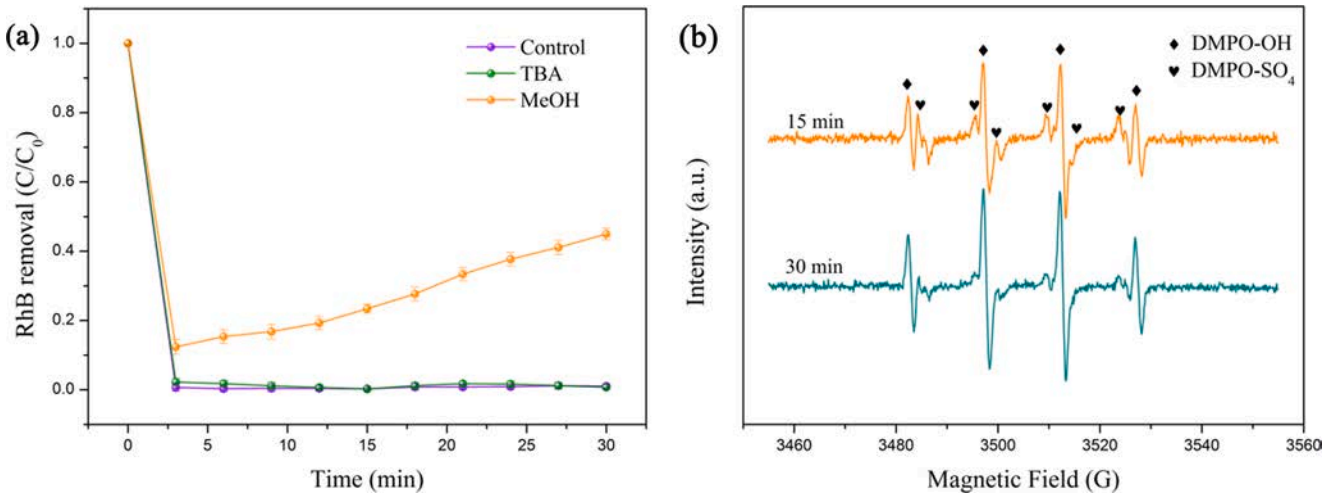

Fig. 9. Radical quenching test (a) and EPR analysis (b).

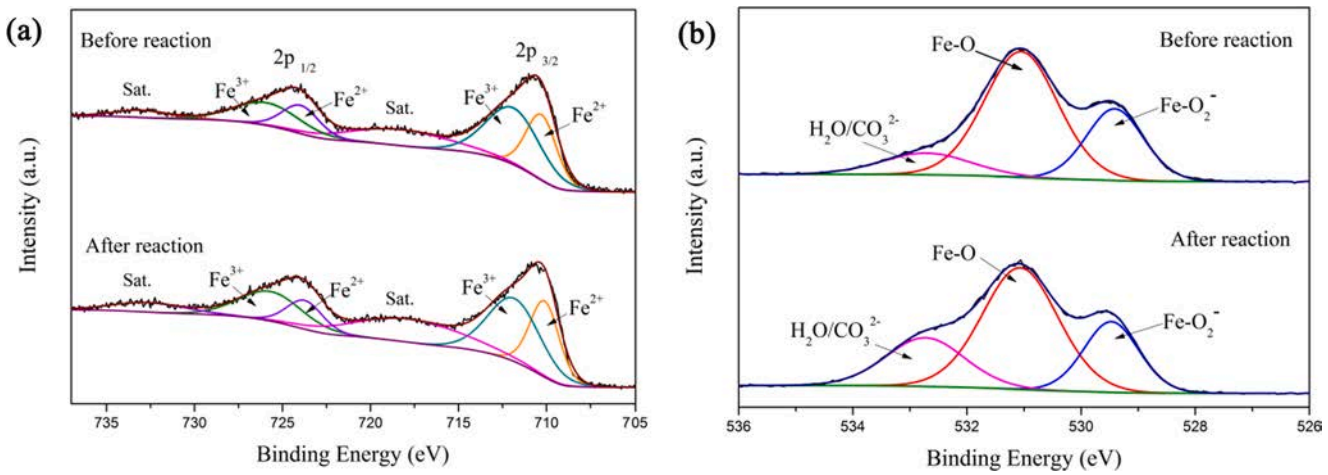

Fig. 10. High-resolution XPS spectrum of Fe 2p (a) and O 1s (b) before and after reaction.

β-FeOOH-12 membrane remained basically unchanged after the 10 cycles of degradation processes, indicating the stability of the as-prepared catalytic membrane, which also explains the limited change in the composition of lattice oxygen (Fe-O_2^-) in β-FeOOH structure. Therefore, it was inferred that the Fe-O bonds on β-FeOOH surface were mainly involved in the PMS activation processes and thus dominated the degradation of the pollutants.

Based on the above analysis, the mechanism of the PVDF/β-FeOOH-12 membrane for pollutants degradation is shown in Fig. 11 and explained in the following equations. Firstly, Fe^{2+} reacted with PMS and was oxidized to Fe^{3+}, and $SO_4^{\cdot-}$ was generated during this process as Eq. (5). Secondly, Fe^{3+} was reduced to Fe^{2+} to accomplish the repair cycle of Fe^{3+}/Fe^{2+} by accepting the electron as Eq. (6) [23,53]. However, owing to the restricted reaction rate, Eq. (6) was often considered as the rate-limiting step [7]. Besides, ·OH was also involved in PMS activation process through Eq. (7). Finally, the organic was partially oxidized and gradually mineralized to H_2O and CO_2 as the reaction progressed.

$$Fe^{2+} + HSO_5^- \rightarrow SO_4^{\cdot-} + Fe^{3+} + OH^- \quad (5)$$

$$Fe^{3+} + HSO_5^- \rightarrow SO_5^{\cdot-} + Fe^{2+} + H^+ \quad (6)$$

$$SO_4^{\cdot-} + {}^{\cdot}OH^- \rightarrow SO_4^{2-} + {}^{\cdot}OH \quad (7)$$

$$Organic + SO_4^{\cdot-}\left(OH + SO_5^{\cdot-}\right) \rightarrow Intermediates \rightarrow CO_2 + H_2O + SO_4^{2-} \quad (8)$$

The intermediate products of the RhB degradation were analyzed and depicted in Figs. S11–S12. In the initial stage of the catalytic oxidation, the side chain alkyl groups of RhB were destroyed and disappeared gradually through dealkylation reaction to generate P1 and P2 with the *m/z* of 359.1. Afterwards, ring-opening reaction was dominated to open benzene ring and formed P3, P4, and P5 (*m/z* = 279.1, 274.3, and 217.2) respectively. Then, the intermediate products were further oxidized to small organic like P6 and P7 (*m/z* = 169.0 and 155.1) under the attack of free radicals. Finally, the RhB was further oxidized and partially mineralized to CO_2 and H_2O as a result.

The comparisons of the separation and degradation performance of the catalytic membranes are summarized in Table S3. After extensive comparisons among the catalytic membranes, we found that most of the studies divided the separation and catalytic oxidation performance into two parts. In this regard, the main characteristic of the membrane, the separation performance was separated from the catalytic degradation performance, and thus, the integrity of the catalytic membrane performance was not fully guaranteed. Besides, the uneven distribution of the heterogeneous catalysts also hindered the further development of catalytic performance. In this study, the merits of the catalytic oxidation and membrane technology were effectively combined by rationally regulating membrane structure via an *in situ* mineralization method. Accordingly, physical size sieving and catalytic oxidation can be employed simultaneously to realize high rejection of oil-in-water emulsions and small organic pollutants degradation. Furthermore, the PVDF/β-FeOOH-12 membrane can achieve high-efficient degradation and separation performance under lower operating pressure, which is

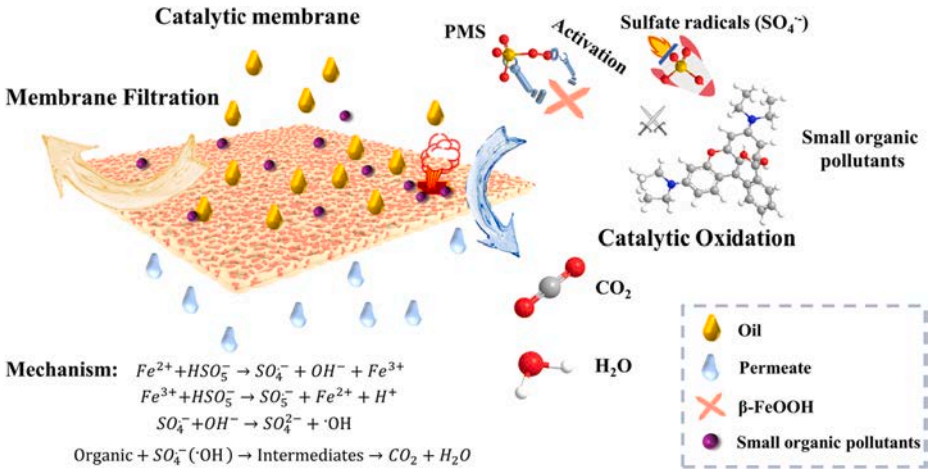

Fig. 11. Mechanism of the PVDF/β-FeOOH-12 membrane for organic pollutants degradation.

more in line with the requirement of green chemistry. Therefore, it is conducive to the further application of the catalytic membrane.

4. Conclusion

In this study, a facile *in situ* mineralization method was employed to achieve the uniform distribution of the heterogeneous catalysts on confined membrane pores. The uniformly distributed β-FeOOH not only optimized the hydrophilicity and structure of the membrane but also enabled favorable catalytic activity for pollutant degradation. Correspondingly, the PVDF/β-FeOOH-12 membrane exhibited favorable catalytic oxidation ability and separation performance under confinement effect provides by tortuous channels in membrane structure. Rapid degradation of small organic pollutants and effective separation of various oil-in-water emulsions can be achieved simultaneously under lower operating pressure compared with other catalytic membrane (Table S3). Radical quenching test and EPR analysis proved that the $SO_4^{\cdot-}$ were the predominant reactive oxygen species in catalytic oxidation process. Besides, the PVDF/β-FeOOH-12 membrane also possessed favorable stability without tedious catalyst recycle process. Therefore, by constructing the uniform distribution of the catalytic reaction sites on confined membrane pore structure, the catalytic performance of the heterogeneous catalysts can be further enhanced, which is conducive to the application in heterogeneous advanced oxidation process.

CRediT authorship contribution statement

Longfei Zhang: Conceptualization, Methodology, Validation, Formal analysis, Investigation, Data curation, Writing – original draft, Writing – review & editing, Visualization. **Na Yang:** Conceptualization, Validation, Supervision, Project administration, Funding acquisition. **Yuhang Han:** Methodology, Formal analysis. **Xiang Wang:** Methodology, Formal analysis. **Luhong Zhang:** Conceptualization, Validation, Supervision, Project administration, Visualization, Funding acquisition, Project administration. **Yongli Sun:** Validation, Supervision, Project administration, Funding acquisition, Project administration. **Bin Jiang:** Methodology, Formal analysis, Project administration, Supervision, Investigation.

Declaration of Competing Interest

The authors declare that they have no known competing financial interests or personal relationships that could have appeared to influence the work reported in this paper.

Acknowledgements

The authors greatly acknowledge the financial support of National Natural Science Foundation of China (22078233).

Appendix A. Supplementary material

Supplementary data to this article can be found online at https://doi.org/10.1016/j.seppur.2021.119684.

References

[1] M.S. Mauter, I. Zucker, F.o. Perreault, J.R. Werber, J.-H. Kim, M. Elimelech, The role of nanotechnology in tackling global water challenges, Nat. Sustain., 1 (2018) 166-175.
[2] B.C. Hodges, E.L. Cates, J.H. Kim, Challenges and prospects of advanced oxidation water treatment processes using catalytic nanomaterials, Nat. Nanotechnol. 13 (2018) 642–650.
[3] Z. Jeirani, C.H. Niu, J. Soltan, Adsorption of emerging pollutants on activated carbon, Rev. Chem. Eng. 33 (2017) 491–522.
[4] L. Zhang, L. Zhang, Y. Sun, B. Jiang, Porous ZrO_2 encapsulated perovskite composite oxide for organic pollutants removal: Enhanced catalytic efficiency and suppressed metal leaching, J. Colloid Interface Sci. 596 (2021) 455–467.
[5] R. Rosal, A. Rodríguez, J.A. Perdigón-Melón, A. Petre, E. García-Calvo, M. J. Gómez, A. Agüera, A.R. Fernández-Alba, Occurrence of emerging pollutants in urban wastewater and their removal through biological treatment followed by ozonation, Water Res. 44 (2010) 578–588.
[6] S. Wacławek, H.V. Lutze, K. Grübel, V.V.T. Padil, M. Černík, D.D. Dionysiou, Chemistry of persulfates in water and wastewater treatment: A review, Chem. Eng. J. 330 (2017) 44–62.
[7] W.-D. Oh, Z. Dong, T.-T. Lim, Generation of sulfate radical through heterogeneous catalysis for organic contaminants removal: Current development, challenges and prospects, Appl. Catal. B 194 (2016) 169–201.
[8] H. Sun, C. Kwan, A. Suvorova, H.M. Ang, M.O. Tadé, S. Wang, Catalytic oxidation of organic pollutants on pristine and surface nitrogen-modified carbon nanotubes with sulfate radicals, Appl. Catal. B 154–155 (2014) 134–141.
[9] X. Liao, F. Wang, F. Wang, Y. Cai, Y. Yao, B.-T. Teng, Q. Hao, L. Shuxiang, Synthesis of (100) surface oriented MIL-88A-Fe with rod-like structure and its enhanced fenton-like performance for phenol removal, Appl. Catal. B 259 (2019), 118064.
[10] N. Zhou, J. Zu, L. Yang, X. Shu, J. Guan, Y. Deng, D. Gong, C. Ding, M.-E. Zhong, Cobalt (0/II) incorporated N-doped porous carbon as effective heterogeneous peroxymonosulfate catalyst for quinclorac degradation, J. Colloid Interface Sci. 563 (2020) 197–206.
[11] Y. Du, W. Ma, P. Liu, B. Zou, J. Ma, Magnetic $CoFe_2O_4$ nanoparticles supported on titanate nanotubes ($CoFe_2O_4$/TNTs) as a novel heterogeneous catalyst for peroxymonosulfate activation and degradation of organic pollutants, J. Hazard. Mater. 308 (2016) 58–66.
[12] J. Ye, C. Li, L. Wang, Y. Wang, J. Dai, Synergistic multiple active species for catalytic self-cleaning membrane degradation of persistent pollutants by activating peroxymonosulfate, J. Colloid Interface Sci. 587 (2021) 202–213.
[13] S. Wang, J. Tian, Q. Wang, F. Xiao, S. Gao, W. Shi, F. Cui, Development of CuO coated ceramic hollow fiber membrane for peroxymonosulfate activation: a highly efficient singlet oxygen-dominated oxidation process for bisphenol a degradation, Appl. Catal. B 256 (2019), 117783.
[14] H. Lin, Q. Fang, W. Wang, G. Li, J. Guan, Y. Shen, J. Ye, F. Liu, Prussian blue/PVDF catalytic membrane with exceptional and stable Fenton oxidation performance for organic pollutants removal, Appl. Catal. B 273 (2020), 119047.
[15] J. Ye, J. Dai, L. Wang, C. Li, Y. Yan, G. Yang, Investigation of catalytic self-cleaning process of multiple active species decorated macroporous PVDF membranes through peroxymonosulfate activation, J. Colloid Interface Sci. 586 (2021) 178–189.
[16] L. Zhang, Y. Zhang, J. Wei, W. Liu, Perovskite $LaFe_xCo_{1-x}O_{3-\lambda}$ deposited SiO_2 catalytic membrane for deeply cleaning wastewater, Chem. Eng. J. 403 (2021), 126386.
[17] Y. Ren, T. Li, W. Zhang, S. Wang, M. Shi, C. Shan, W. Zhang, X. Guan, L. Lv, M. Hua, B. Pan, MIL-PVDF blend ultrafiltration membranes with ultrahigh MOF loading for simultaneous adsorption and catalytic oxidation of methylene blue, J. Hazard. Mater. 365 (2019) 312–321.
[18] H. Zhang, X. Wang, Y. Li, K. Zuo, C. Lyu, A novel MnOOH coated nylon membrane for efficient removal of 2,4-dichlorophenol through peroxymonosulfate activation, J. Hazard. Mater. 414 (2021), 125526.
[19] Y. Zhang, H. Zhang, S. Tian, L. Zhang, W. Li, W. Wang, X. Yan, N. Han, X. Zhang, The photocatalysis-enhanced TiO_2@HPAN membrane with high TiO_2 surface content for highly effective removal of cationic dyes, Langmuir 37 (2021) 9415–9428.
[20] C. Yang, N. Han, W. Zhang, W. Wang, W. Li, B. Xia, C. Han, Z. Cui, X. Zhang, Adhesive-free in situ synthesis of a coral-like titanium dioxide@poly(phenylene sulfide) microporous membrane for visible-light photocatalysis, Chem. Eng. J. 374 (2019) 1382–1393.
[21] Y. Chen, G. Zhang, H. Liu, J. Qu, Confining free radicals in close vicinity to contaminants enables ultrafast Fenton-like processes in the interspacing of MoS_2 membranes, Angew. Chem. Int. Ed. Engl. 58 (2019) 8134–8138.
[22] S. Zhang, T. Hedtke, Q. Zhu, M. Sun, S. Weon, Y. Zhao, E. Stavitski, M. Elimelech, J.-H. Kim, Membrane-confined iron oxychloride nanocatalysts for highly efficient heterogeneous fenton water treatment, Environ. Sci. Technol. 55 (2021) 9266–9275.
[23] Z. He, S. Mahmud, S. Zhao, Y. Yang, L. Zhu, Y. Zhao, Q. Zeng, Z. Xiong, C. Hu, Hierarchically active poly(vinylidene fluoride) membrane fabricated by in situ generated zero-valent iron for fouling reduction, ACS Appl. Mater. Interfaces 12 (2020) 10993–11004.
[24] N. Li, X. Lu, M. He, X. Duan, B. Yan, G. Chen, S. Wang, Catalytic membrane-based oxidation-filtration systems for organic wastewater purification: A review, J. Hazard. Mater. 414 (2021), 125478.
[25] Z. Chen, J. Wang, X. Duan, Y. Chu, X. Tan, S. Liu, S. Wang, Facile fabrication of 3D ferrous ion crosslinked graphene oxide hydrogel membranes for excellent water purification, Environ. Sci. Nano 6 (2019) 3060–3071.
[26] T. Ma, L. Liu, B. Meng, J. Gao, S. Wang, S. Liu, Heterogeneous activation of peroxymonosulfate via a Ag-$La_{0.8}Ca_{0.2}Fe_{0.94}O_{3-\delta}$ perovskite hollow fibre membrane reactor for dye degradation, Sep. Purif. Technol. 211 (2019) 298–302.
[27] H. Wu, X. Xu, L. Shi, Y. Yin, L.C. Zhang, Z. Wu, X. Duan, S. Wang, H. Sun, Manganese oxide integrated catalytic ceramic membrane for degradation of organic pollutants using sulfate radicals, Water Res. 167 (2019), 115110.
[28] J. Ye, C. Li, L. Wang, Y. Yan, Y. Wang, J. Dai, MOFs derived 3D sea urchin-like carbon frameworks loaded on PVDF membranes as PMS activator for highly efficient bisphenol A degradation, Sep. Purif. Technol. 258 (2021), 117669.
[29] J. Kang, H. Zhang, X. Duan, H. Sun, X. Tan, S. Liu, S. Wang, Magnetic Ni-Co alloy encapsulated N-doped carbon nanotubes for catalytic membrane degradation of emerging contaminants, Chem. Eng. J. 362 (2019) 251–261.

[30] H. Shan, X. Dong, X. Cheng, Y. Si, J. Yu, B. Ding, Highly flexible, mesoporous structured, and metallic Cu-doped C/SiO_2 nanofibrous membranes for efficient catalytic oxidative elimination of antibiotic pollutants, Nanoscale 11 (2019) 14844–14856.
[31] N. Li, G. Chen, J. Zhao, B. Yan, Z. Cheng, L. Meng, V. Chen, Self-cleaning PDA/ZIF-67@PP membrane for dye wastewater remediation with peroxymonosulfate and visible light activation, J. Membr. Sci. 591 (2019), 117341.
[32] Y. Bao, Y.S. Tay, T.-T. Lim, R. Wang, R.D. Webster, X. Hu, Polyacrylonitrile (PAN)-induced carbon membrane with in-situ encapsulated cobalt crystal for hybrid peroxymonosulfate oxidation-filtration process: Preparation, characterization and performance evaluation, Chem. Eng. J. 373 (2019) 425–436.
[33] H. Lv, H. Niu, X. Zhao, Y. Cai, F. Wu, Carbon zero-valent iron materials possessing high-content fine Fe0 nanoparticles with enhanced microelectrolysis-Fenton-like catalytic performance for water purification, Appl. Catal. B 286 (2021), 119940.
[34] Z. Zhu, C. Ji, L. Zhong, S. Liu, F. Cui, H. Sun, W. Wang, Magnetic Fe–Co crystal doped hierarchical porous carbon fibers for removal of organic pollutants, J. Mater. Chem. A 5 (2017) 18071–18080.
[35] Q. Wu, H. Yang, L. Kang, Z. Gao, F. Ren, Fe-based metal-organic frameworks as Fenton-like catalysts for highly efficient degradation of tetracycline hydrochloride over a wide pH range: Acceleration of Fe(II)/Fe(III) cycle under visible light irradiation, Appl. Catal. B 263 (2020), 118282.
[36] J. Li, L. Zhao, R. Zhang, H.H. Teng, L.P. Padhye, P. Sun, Transformation of tetracycline antibiotics with goethite: Mechanism, kinetic modeling and toxicity evaluation, Water Res. 199 (2021), 117196.
[37] S. Zheng, H. Chen, X. Tong, Z. Wang, J.C. Crittenden, M. Huang, Integration of a photo-fenton reaction and a membrane filtration using CS/PAN@FeOOH/g-C_3N_4 electrospun nanofibers: synthesis, characterization, self-cleaning performance and mechanism, Appl. Catal. B: Environ. 281 (2021), 119519.
[38] X. Wang, W. Lu, Z. Zhao, H. Zhong, Z. Zhu, W. Chen, In situ stable growth of β-FeOOH on g-C_3N_4 for deep oxidation of emerging contaminants by photocatalytic activation of peroxymonosulfate under solar irradiation, Chem. Eng. J. 400 (2020), 125872.
[39] C. Lyu, D. He, Z. Mou, X. Yang, Synergetic activation of peroxymonosulfate by MnO_2-loaded β-FeOOH catalyst for enhanced degradation of organic pollutant in water, Sci. Total Environ. 693 (2019), 133589.
[40] L. Zhang, X. Yang, B. Jiang, Y. Sun, Z. Gong, N. Zhang, S. Hou, J. Li, N. Yang, Superhydrophilic and underwater superoleophobic Ti foam with robust nanoarray structures of TiO_2 for effective oil-in-water emulsion separation, Sep. Purif. Technol. 252 (2020), 117437.
[41] N. Zhang, N. Yang, L. Zhang, B. Jiang, Y. Sun, J. Ma, K. Cheng, F. Peng, Facile hydrophilic modification of PVDF membrane with Ag/EGCG decorated micro/nanostructural surface for efficient oil-in-water emulsion separation, Chem. Eng. J. 402 (2020), 126200.
[42] K. Saha, J. Deka, S. Hens, S. Saikia, K. Raidongia, Chemical reactions under the nanofluidic confinement of reconstructed lamellar membranes, J. Mater. Chem. A 6 (2018) 22931–22939.
[43] L. Zhang, Y. He, L. Ma, J. Chen, Y. Fan, S. Zhang, H. shi, Z. Li, P. Luo, Hierarchically stabilized PAN/β-FeOOH nanofibrous membrane for efficient water purification with excellent antifouling performance and robust solvent resistance, ACS Appl. Mater. Interfaces, 11 (2019) 34487-34496.
[44] X. Zhao, L. Cheng, N. Jia, R. Wang, L. Liu, C. Gao, Polyphenol-metal manipulated nanohybridization of CNT membranes with FeOOH nanorods for high-flux, antifouling and self-cleaning oil/water separation, J. Membr. Sci. 600 (2020), 117857.
[45] M. Wang, Z. Xu, Y. Hou, P. Li, H. Sun, Q.J. Niu, Photo-Fenton assisted self-cleaning hybrid ultrafiltration membranes with high-efficient flux recovery for wastewater remediation, Sep. Purif. Technol. 249 (2020), 117159.
[46] B. Li, Y. Yun, M. Wang, C. Li, W. Yang, J. Li, G. Liu, Superhydrophobic polymer membrane coated by mineralized β-FeOOH nanorods for direct contact membrane distillation, Desalination 500 (2021), 114889.
[47] A. Xie, J. Cui, J. Yang, Y. Chen, J. Dai, J. Lang, C. Li, Y. Yan, Photo-Fenton self-cleaning membranes with robust flux recovery for an efficient oil/water emulsion separation, J. Mater. Chem. A 7 (2019) 8491–8502.
[48] W. Liu, S. Xiang, X. Liu, B. Yang, Underwater superoleophobic surface based on silica hierarchical cylinder arrays with a low aspect ratio, ACS Nano (2020).
[49] Y. Lv, C. Zhang, A. He, S.-J. Yang, G.-P. Wu, S.B. Darling, Z.-K. Xu, Photocatalytic nanofiltration membranes with self-cleaning property for wastewater treatment, Adv. Funct. Mater. 27 (2017) 1700251.
[50] X. Cheng, Z. Sun, X. Yang, Z. Li, Y. Zhang, P. Wang, H. Liang, J. Ma, L. Shao, Construction of superhydrophilic hierarchical polyacrylonitrile nanofiber membranes by in situ asymmetry engineering for unprecedently ultrafast oil–water emulsion separation, J. Mater. Chem. A 8 (2020) 16933–16942.
[51] J. Ye, Y. Wang, Z. Li, D. Yang, C. Li, Y. Yan, J. Dai, 2D confinement freestanding graphene oxide composite membranes with enriched oxygen vacancies for enhanced organic contaminants removal via peroxymonosulfate activation, J. Hazard. Mater. 417 (2021), 126028.
[52] P. Shao, J. Tian, F. Yang, X. Duan, S. Gao, W. Shi, X. Luo, F. Cui, S. Luo, S. Wang, Identification and regulation of active sites on nanodiamonds: establishing a highly efficient catalytic system for oxidation of organic contaminants, Adv. Funct. Mater. 28 (2018) 1705295.
[53] M. Ahmad, X. Quan, S. Chen, H. Yu, Tuning Lewis acidity of MIL-88B-Fe with mix-valence coordinatively unsaturated iron centers on ultrathin Ti3C2 nanosheets for efficient photo-Fenton reaction, Appl. Catal. B 264 (2020), 118534.